

Article

Magnetic Properties and Initiation of Biogenic Reefs in Xisha Islands, South China Sea, at the Oligo–Miocene Boundary

Yibing Li ¹ , Xinyu Liu ², Weiwei Chen ¹ and Liang Yi ^{1,*} 

¹ State Key Laboratory of Marine Geology, Tongji University, Shanghai 200092, China; yibing_li@163.com (Y.L.); sww@tongji.edu.cn (W.C.)

² China National Offshore Oil Corporation Ltd., Hainan Branch, Haikou 570100, China; liuxy5@cnooc.com.cn

* Correspondence: yiliang@tongji.edu.cn

Abstract: Biogenic reefs and carbonate platforms are valuable natural resources, playing an important role in modulating the global climate and in carbon cycles through biological processes. Biogenic reefs in the Xisha (Paracel) Islands began in the late Oligocene and covaried with the deep-sea basin of the South China Sea and with the aeolian deposit in the Chinese Loess Plateau. Core XK-1 was drilled into the Xisha Islands to their granitic base and well dated by magnetostratigraphy, offering an opportunity to reveal the details of how the Xisha reefs initiated. In this report, the lower section of the biogenic reefs (23.0–24.5 Ma) was sampled for studying magnetic properties. The main results are as follows: (1) magnetic minerals in the XK-1 biogenic reefs are dominated by low-coercivity and relatively coarse-grained magnetite; (2) the variabilities of magnetic parameters can be clustered into two sections around 23.6 Ma, and the differences between the two units are evident both in the amplitudes and the means; and (3) changes in the concentration-dependent magnetic parameters can be well correlated with the records of global deep-sea oxygen and carbon isotopes, and the sea level during the Oligo–Miocene boundary. Based on these results, a close link was inferred between biogenic reef evolution in the Xisha Islands and global climate change. This link likely highlights the covariation or the dominant role of the Asian monsoon in biogenic reefs and involves different responses to global temperature, CO₂, and sea-level changes on various timescales. Therefore, we proposed that the origin of biogenic reefs in the Xisha Islands was likely paced by orbital obliquity from a long-term perspective.

Keywords: biogenic reefs; Xisha (Paracel) Islands; climate change; late Oligocene; early Miocene; orbital forcing



Citation: Li, Y.; Liu, X.; Chen, W.; Yi, L. Magnetic Properties and Initiation of Biogenic Reefs in Xisha Islands, South China Sea, at the Oligo–Miocene Boundary. *J. Mar. Sci. Eng.* **2021**, *9*, 1031. <https://doi.org/10.3390/jmse9091031>

Academic Editor: Ernesto Weil

Received: 13 August 2021

Accepted: 15 September 2021

Published: 19 September 2021

Publisher's Note: MDPI stays neutral with regard to jurisdictional claims in published maps and institutional affiliations.



Copyright: © 2021 by the authors. Licensee MDPI, Basel, Switzerland. This article is an open access article distributed under the terms and conditions of the Creative Commons Attribution (CC BY) license (<https://creativecommons.org/licenses/by/4.0/>).

1. Introduction

Tropical reefs are composed of corals, algae, and other reef-building organisms with an anti-wave structure. Accounting for a quarter of the global annual carbonate production [1,2], biogenic reefs are critical in revealing the links and interactions between mid- and high-latitude environmental processes from the perspective of tropical oceans. However, they are all suffering a continuous decline and bleaching in the context of global warming and ocean acidification [3–5]. To overturn this decline and bleaching and to maintain ecological function again, the full cooperation of science, society, and policy in protecting coral reefs is necessary around the world [6], and due to the unclear response of coral reefs to global changes, there are many uncertainties in predicting the future of coral reefs. For example, combining human social systems with factors of forestry, freshwater lakes, fisheries, agricultural abandonment, and climate change in box models [7–13], an increase in complexity and in prediction uncertainty is evident [14].

Modern observations cover the past several decades, and these data have great limitations in effectively developing models for coral reefs. For example, the changing hydrochemical characteristics in geological timescales may control coral evolution [15], and

during a warm period of global climate in the middle Miocene [16], coral reefs largely developed in the Western Pacific [17,18]. Hence, it is speculated that coral reefs in different geological periods have different responses to global climate change, and studying the long-term sequence of coral reefs can provide a useful reference, supplementary to modern observations.

The South China Sea is the largest marginal sea in Asia (Figure 1). Numerous coral reefs developed in the Eocene and early Oligocene in the south [19–23], while in the north, reefs mainly formed on uplifted fault blocks or on volcanic seamounts [17,24] starting from the late Oligocene [18,25]. These carbonate deposits not only relate to the evolution of the South China Sea but also serve as a valuable natural resource and precious heritage. Lithological studies suggest that these carbonate deposits in both the southern and northern parts of the South China Sea are comparable with each other [26–28], while few geochronological investigations from a paleoenvironmental and palaeoclimatological perspective have been performed (e.g., [18,29,30]), precluding our understanding of the initiation and development of these biogenic reefs. Moreover, although commonly used proxies, such as geochemical components and carbonate $\delta^{18}\text{O}$ and $\delta^{13}\text{C}$, are significantly influenced by diageneses and dolomitization (e.g., [31]), the magnetic properties of biogenic reefs are useful as a paleoenvironmental proxy in the South China Sea and the South Pacific (e.g., [32,33]). Those magnetic particles are mainly magnetite in the pseudo-single domain (PSD), which could be trapped during coral growth. In addition, aeolian deposits were found on the top of biogenic reefs at several sites in the Xisha (Paracel) Islands, suggesting an evident influence of the Asian monsoon in this region [26,34,35]. Therefore, this study aims to reveal the evolution of biogenic reefs in the Xisha (Paracel) Islands and how this carbonate bank responded to global climate change during the Oligo–Miocene transition. To this end, detailed magnetic properties are investigated on core XK-1, drilled from Shidao Island in the Xisha (Paracel) Islands (Figure 1).

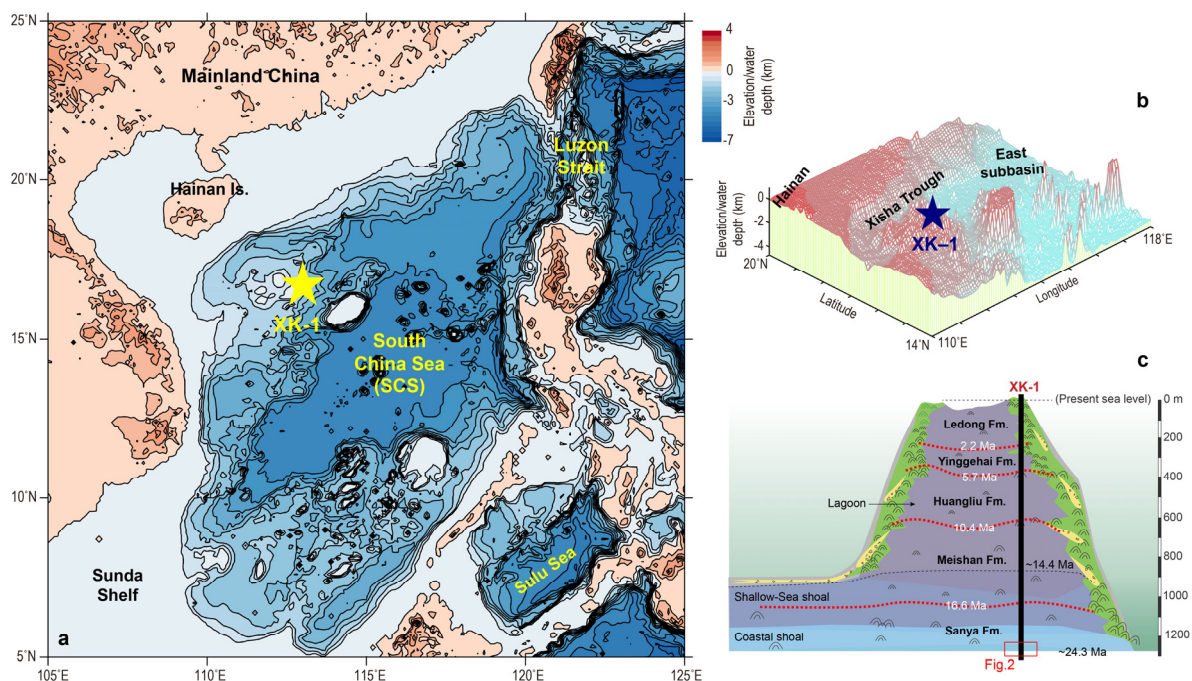


Figure 1. Study area and the location of core XK-1. (a) The South China Sea (SCS). (b) Topography of Xisha (Paracel) Islands. (c) The skeleton of the Shidao Island with the five formations identified in regional studies. The age boundary of each formation was from [18], and the skeleton (c) was modified from previous reports [26,34,35]. The base map data were generated using the open and free software DIVA-GIS 7.5 (<http://www.diva-gis.org/>, accessed on 10 September 2021).

2. Materials and Methods

2.1. Core XK-1

The Xisha (Paracel) Islands are located in the northwest of the South China Sea (Figure 1a), and the total area of coral reefs in this region is about 1836 km². The Xisha Uplift is the main structural element in the study area, which subsided around the Oligo–Miocene boundary [36,37]. Since then, tropical biogenic reefs have developed, forming the Xisha carbonate bank [18,30].

Core XK-1 was drilled to the bottom of the Xisha carbonate platform on Shidao Island in the Xuande Atoll, Xisha (Paracel) Islands (16°50′45″ N, 112°20′50″ E; Figure 1b), by the China National Offshore Oil Corporation in 2012–2013. The total length of the core was 1268 m, with an average recovery rate of 80%. Based on sedimentary facies, five lithological units were identified (Figure 1c): Sanya, Meishan, Huangliu, Yinggehai, and Ledong Formations (Fms.) from bottom to top [38,39]. The ages of each formation are estimated as 2.2 Ma, 5.7 Ma, 10.4 Ma, 16.6 Ma, and 24.3 Ma, respectively [18,25,32,40].

The Sanya Fm. (1258–1032 m) contains a thick dolomitic reef with some bioclastic limestone in the upper part, alternating reefal and bioclastic limestone in the middle, and brownish breccia and coral reefs in the bottom (Figure 2). Fossils of *Actinacis* and *Spiroclypeus* were found at 1245 m and 1255 m in core XK-1, respectively [41], supporting the estimate that these biogenic reefs date back to the late Oligocene [18]. Besides the two fossils, red algae, including *Lithoporella melobesioides*, *Lithoporella minus*, *Neogoniolithon*, and *Mesophyllum*, and benthic foraminifera, including *Amphistegina lessonii*, *Amphistegina lobifera*, and *Spiroclypeus* were also found in the lower part of the Sanya Fm. [41].

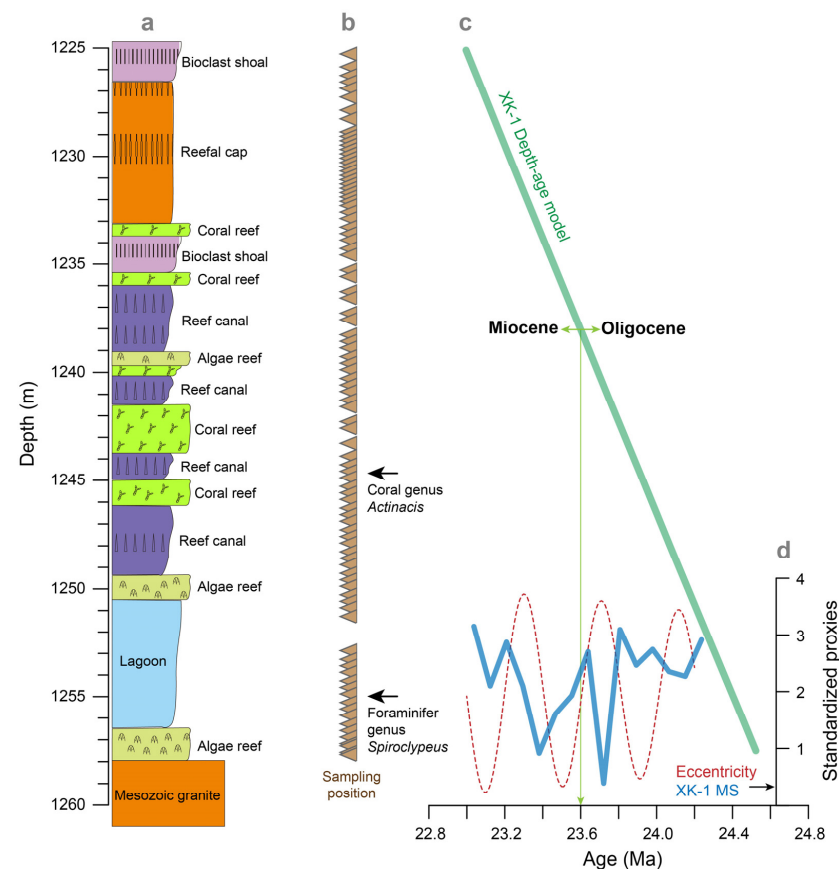


Figure 2. Profile of the studied section of core XK-1. (a) Lithological changes. (b) Sampling position. (c) The preliminary age–depth model of core XK-1. (d) Comparison between orbital eccentricity on 405 kyr band and magnetic susceptibility (MS) of core XK-1 on the preliminary timescale. The data presented in (c,d) were from Reference [18].

The depositional rates of the Sanya Fm. are 10–30 m/Myr, lower than other parts of the core [18]. Due to the low sampling rate (1–3 m) and the low magnetic susceptibility [18,40], there are lots of uncertainties in the astronomical age model in the lower part of core XK-1. Considering the relatively stable depositional processes of biogenic reefs in the South China Sea in the Neogene [30] and the reliability of magnetostratigraphy [25], which was supported by the identified fossils (*Actinacis* and *Spiroclypeus*), we employed the preliminary age model in this study (Figure 2c) to reveal the relationship between the initiation of biogenic reefs in the South China Sea and global climate change.

2.2. Measurements

Focusing on the interval of the Oligo–Miocene transition, the lower part of the Sanya Fm. in core XK-1 was sampled (1258–1225 m), spanning 24.5–23.0 Ma according to the preliminary age model [18]. A total of 93 samples were collected for the magnetic measurements (Figure 2).

All samples were placed in standard 8 cm³ plastic cubic boxes. Magnetic susceptibility (MS) was measured using an AGICO MFK1–FA Multi-Frequency Kappabridge magnetic susceptibility meter by [18]; however, due to low values close to the instrument background, MS data were not included in this study.

Anhyseretic remanent magnetization (ARM) was imparted onto the samples using a peak alternating field (AF) of 100 mT and a direct biasing field of 0.05 mT using a 2G Enterprises SQUID magnetometer with inline AF coils, and then, the susceptibility of ARM (χ_{ARM}) was calculated as ARM/0.05 mT. Isothermal remanent magnetization (IRM) was produced with a 2-G Enterprises model 660 pulse magnetizer successively in pulsed fields of 1 T (saturated IRM, SIRM), -0.1 T (IRM_{-0.1T}), and -0.3 T (IRM_{-0.3T}). The hard isothermal remanent magnetization (HIRM), S_{ratio} , and L_{ratio} , were calculated using the following equations [42]:

$$\text{HIRM} = \frac{\text{SIRM} - \text{IRM}_{-0.3\text{T}}}{2}; S_{\text{ratio}} = \frac{\text{IRM}_{-0.3\text{T}}}{\text{SIRM}} \times 100\%; L_{\text{ratio}} = \frac{\text{SIRM} - \text{IRM}_{-0.3\text{T}}}{\text{SIRM} - \text{IRM}_{-0.1\text{T}}}$$

Hysteresis loop and first-order reversal curve (FORC) analyses were conducted on representative samples using a Princeton Measurements Inc. MicroMag 3900 Vibrating Sample Magnetometer (VSM). A peak field of 1 T was set for hysteresis loops, and saturation magnetization (Ms), saturation remanence (Mrs), coercive force (Bc), and the coercivity of the remanence (Bcr) were determined from the hysteresis loops [42] after they were corrected using the data between 0.7 and 1.0 T. Setting a peak field of 1.0 T and an interval of 3.2 mT, FORC diagrams (125 lines) were produced using FORCme software [43,44] with a smoothing factor of 11. These measurements were conducted at the Paleomagnetism and Geochronology Lab (PGL), Institute of Geology and Geophysics, Chinese Academy of Sciences.

Due to the extremely low content of magnetic minerals [40], high-resolution magnetic scanning was conducted on a slice (1239 m) to reveal the occurrence state of magnetic particles in biogenic reefs, at Charles University in Prague, Czech Republic [45]. Due to low remanence, the sample was first magnetized using a Magnetic Measurements Pulse Magnetizer (MMPM 10) with a field of 3 T. Then, the sample surface was scanned to reproduce the magnetic field of the sample. The sensitivity of the magnetic probe was 0.01 μT , the distance between the probe and the sample was <0.1 mm, and the spatial resolution was 200 μm .

3. Results

3.1. Changes in Magnetic Parameters

χ_{ARM} is usually sensitive to single-domain (SD) grains [46,47], and SIRM can be used to infer magnetic particles excluding the influence of superparamagnetic (SP) grains [48]. The values of χ_{ARM} and SIRM are $0.16\text{--}9.35 \times 10^{-8} \text{ m}^3/\text{kg}$ and $6.0\text{--}1310 \times 10^{-3} \text{ Am}^2/\text{kg}$, respectively (Figure 3), inferring a low content of magnetic minerals in biogenic reefs.

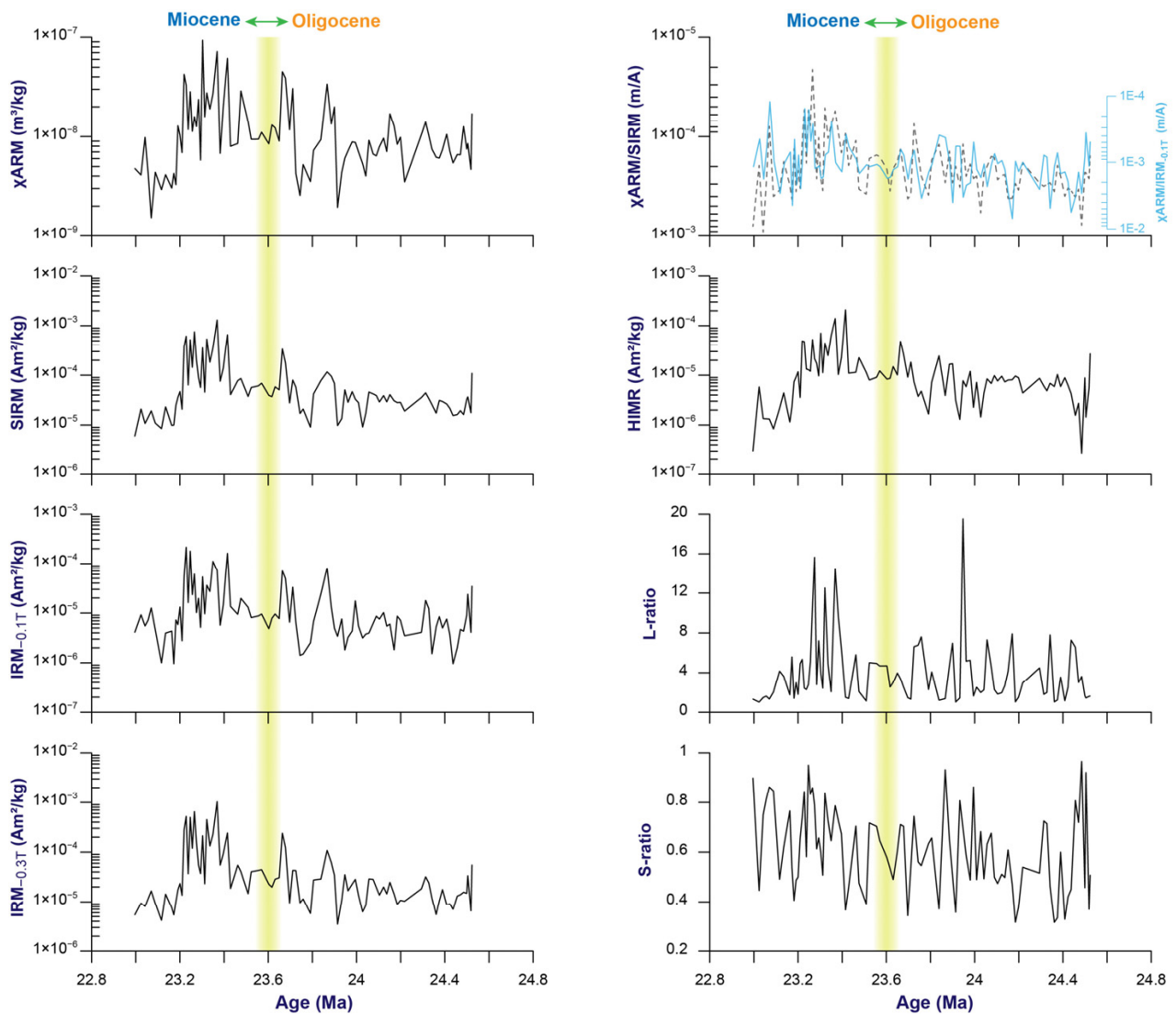


Figure 3. Changes in the magnetic parameters of core XK-1.

Low L_{ratio} values with a high standard deviation (3.96 ± 3.33), close to those in deep-sea sediments in the western Pacific [49], indicate the dominance of low-coercivity magnetic minerals, while low S_{ratio} values (0.61 ± 0.17) might infer the contribution of high-coercivity minerals in biogenic reefs (Figure 3). However, a low concentration of magnetic minerals and a high $CaCO_3$ content may introduce large uncertainties into magnetic measurements. For example, the relationship between the magnetic parameters are more discrete (Figure 4) than those in other sediments (e.g., [49–51]). Considering that the concentration-dependent magnetic parameters (χ_{ARM} and IRMs) have similar variations throughout the studied section (Figure 3), it is inferred that the discrete relationship between the magnetic parameters (Figure 4) may introduce large uncertainties into calculations. Therefore the difference between L_{ratio} and S_{ratio} does not indicate the dominance of high-coercivity magnetic minerals in biogenic reefs of core XK-1.

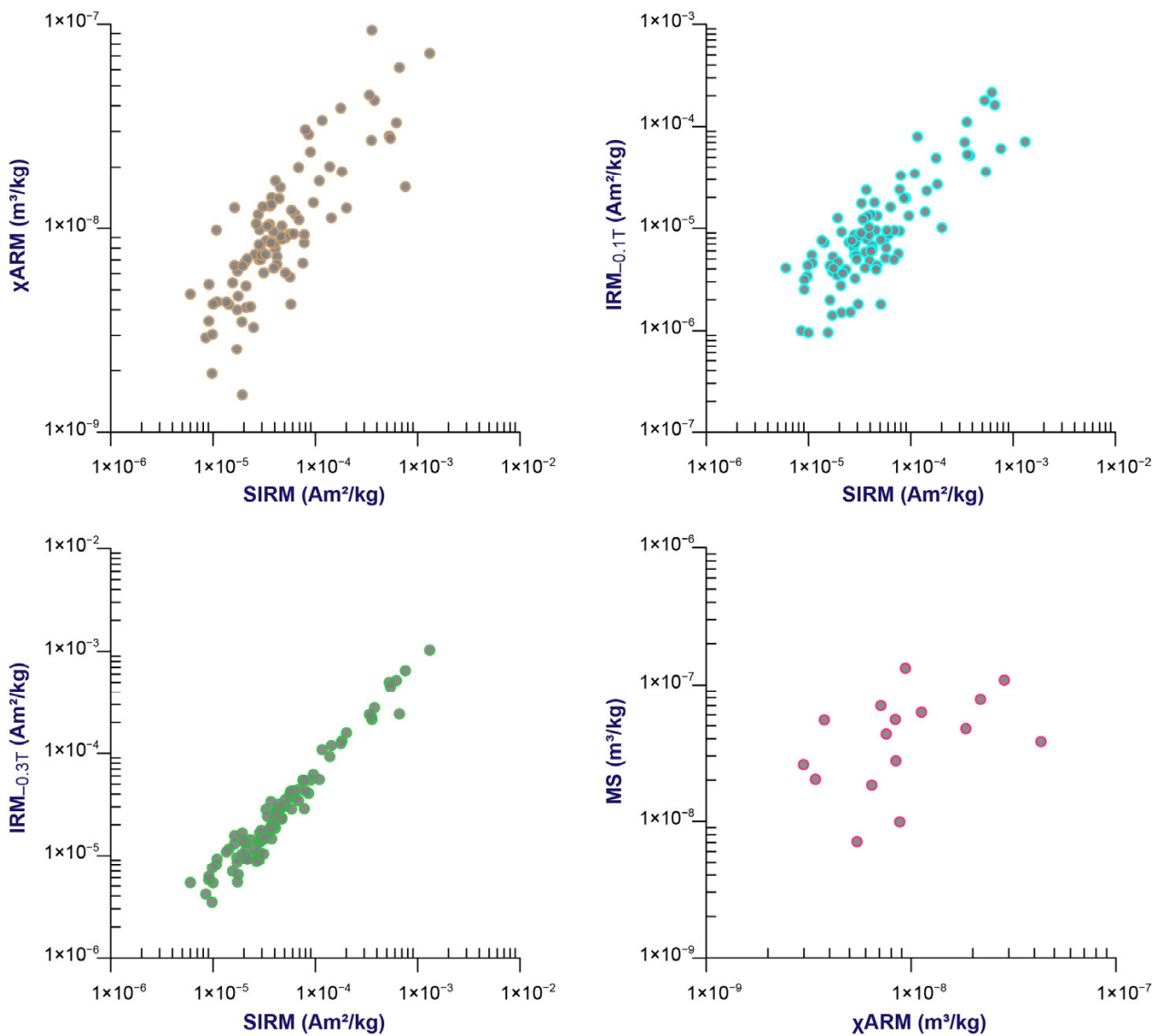


Figure 4. Relationship between the magnetic parameters of core XK-1.

These magnetic variabilities can be generally divided into two units (Figure 3). In specific, for the upper part, the concentration-dependent magnetic parameters (χ ARM and IRMs) have a large average, while for the low part, these records vary greatly but with lower values. By a one-way analysis of variance (ANOVA), the difference of all parameters (χ ARM and IRMs) between the two units is statistically significant ($p < 0.05$), confirming a shift of the changes in magnetic parameters around 23.6 Ma. In addition, the difference in the relationships is not evident (Figure 4), inferring that the source and/or properties of magnetic minerals in biogenic reefs in core XK-1 are similar across the Oligo-Miocene transition.

3.2. Magnetic Minerals and the Proxy

Rock magnetic analysis shows that there are high levels of noise in the hysteresis loops for most of the samples (Figure 5a), and only one obtains a smooth curve (Figure 5b), demonstrating the significant influence of low magnetic minerals and high CaCO_3 content. For the smoothed loop (Figure 5b), it is closed above 200 mT, with B_c and B_{cr} of 11 mT and 52 mT, respectively. On the Day plot, these data are distributed within the lower part of the PSD range. The large vertical spread and wide horizontal spread of the contours in the FORC diagram (Figure 5c) indicate that magnetostatic interactions are evident [52,53],

and the bulk of the coercivity distribution lies in the 5–40 mT range, with peaks at ~10 mT. All of these magnetic properties agree well with those in the upper part of core XK-1 [40], possibly inferring the dominance of detrital magnetite in biogenic reefs.

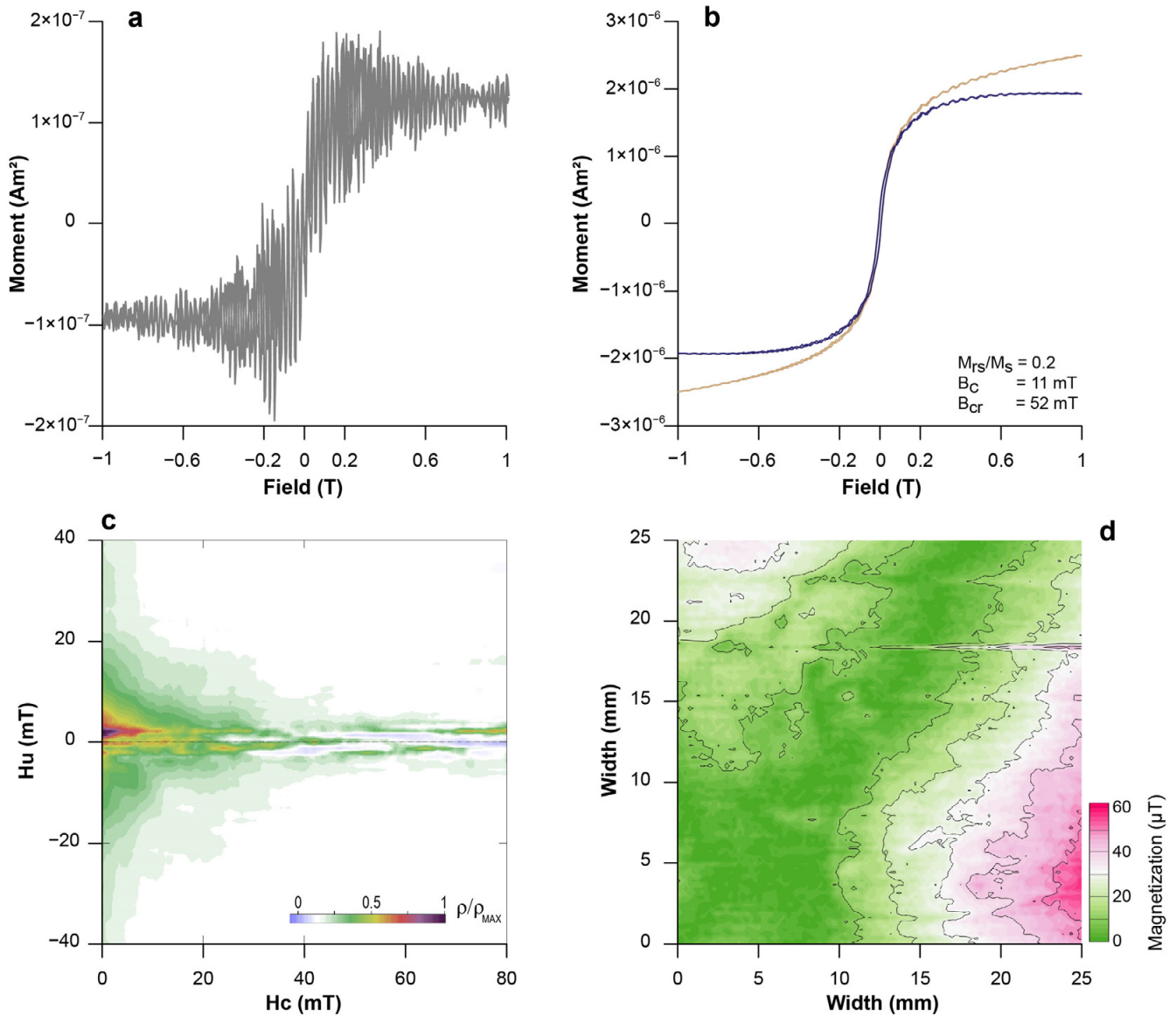


Figure 5. Magnetic properties of biogenic reefs in core XK-1. (a) Hysteresis loops at 1256 m. (b) Hysteresis loops at 1239 m. (c) FORC diagram at 1239 m with a smoothing factor of 9. (d) Scanning result of the sample at 1239 m with a 200- μm interval. Note that hysteresis loop measurements were taken of 11 samples in total, and, since the other 9 samples had a similar loop with (a), these loops are not shown in the figure.

Although detrital minerals are not evident in slice samples under a microscope and most of them were identified by SEM images and energy spectrum analysis (e.g., [54]), high-resolution magnetic scanning can provide useful information about the distribution of magnetic minerals in biogenic reefs [40]. As shown (Figure 5d), the magnetic field of the sample surface is generally weak in the middle part and relatively high at the lower right corner. It is suggested that the content of magnetic minerals in biogenic reefs can be used to indicate the growth intensity [18,30], since magnetic minerals may be enclosed during growth. The relationship is as follows: the greater the magnetic parameters, the higher the concentration of magnetic minerals and the stronger the growing (deposition) processes of biogenic reefs. This case is similarly reported in the Tahiti coral reef in the Southern

Pacific, and magnetite particles were locked in biogenic reefs by biological (microbial) processes [33].

Based on these magnetic properties and the high similarity between the concentration-dependent magnetic parameters (χ_{ARM} and IRMs), a magnetic proxy (MagXK) indicating the growing process of biogenic reefs in core XK-1 was derived (Figure 6a) by a principle component analysis on χ_{ARM} and IRMs. As a result, the MagXK inherits a similar pattern of four magnetic parameters, accounting for 87.8% of variance in total (Table 1), and varies with some cycles (Figure 6b). For other components with a much lower eigenvalue (Table 1), they are not included in analysis. By a wavelet analysis, these cycles can be identified as 40–50 kyr, 100–200 kyr, and 400–500 kyr, which are generally correlated to the periodicities of Earth’s orbits and discussed below.

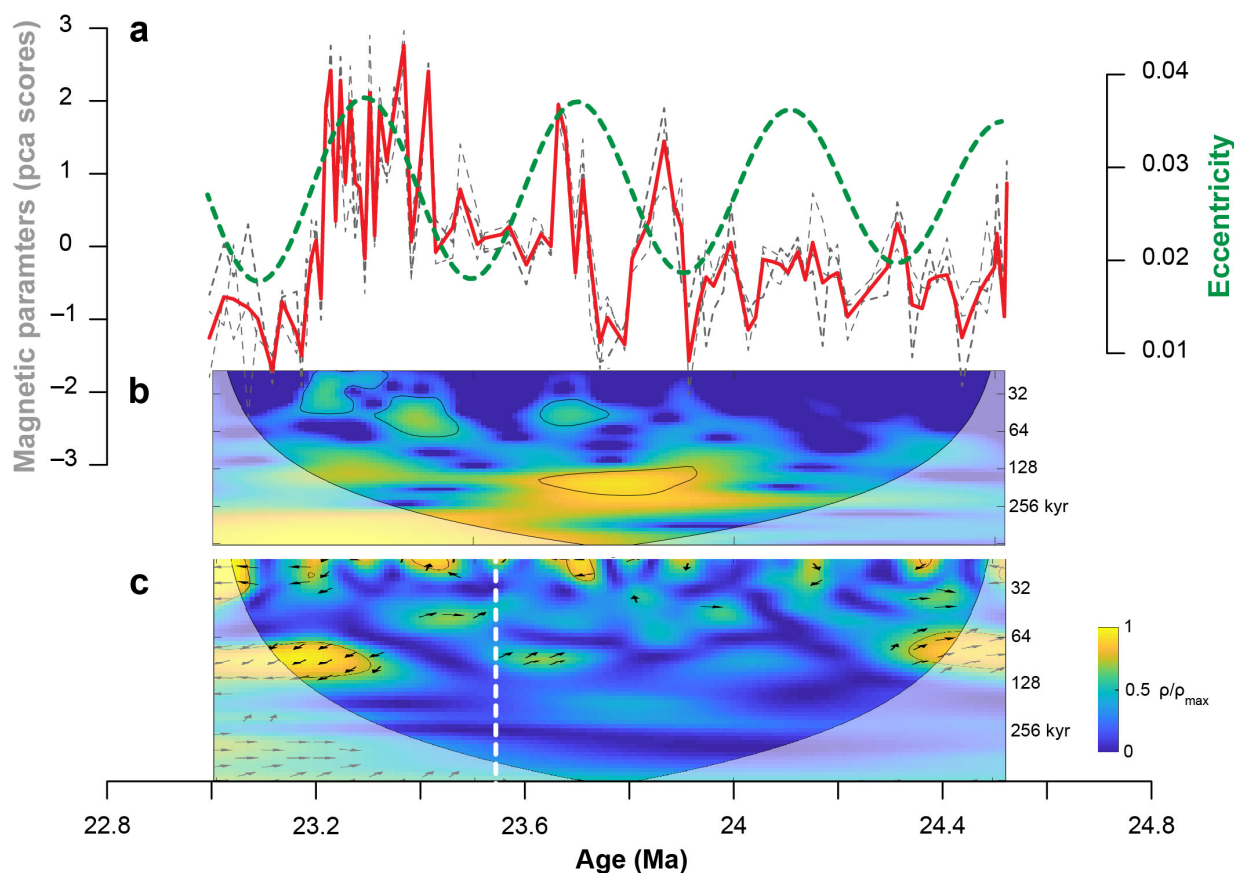


Figure 6. Magnetic proxy (MagXK) of biogenic reefs in core XK-1. (a) MagXK (red bold line) with magnetic parameters (dashed thin lines), versus eccentricity on a 405 kyr band (dashed bold line) [55]. (b) The evolution spectrum of the MagXK. (c) The squared wavelet coherence [56] between MagXK and eccentricity. The thick black contour designates the 5% significance level against red noise, and the cone of influence (COI) where edge effects might distort the picture is shown as a lighter shade. Arrows: in-phase pointing right, anti-phase pointing left.

Table 1. Results of a principal component analysis of magnetic proxies.

Component ¹	Extraction Sums of Squared Loadings		
	Total	% of Variance	Cumulative %
MagXK	3.51	87.77	83.77
	0.25	6.27	94.03
Not included	0.22	5.39	99.42
	0.02	0.58	100

¹ Four concentration-dependent magnetic parameters (χ_{ARM} and IRMs) were analyzed and are shown in Figure 6.

4. Discussion

Biogenic reefs account for a quarter of global annual carbonate production [1,2]. However, these reefs are suffering a continuous decline and bleaching due to global warming and ocean acidification [3–5]. Five principals are critical in the development of carbonate platforms (e.g., [17,57–60]): carbonate production, tectonic activities, sea-level changes, terrigenous material inputs, and paleoceanography. Considering that each principal usually covaries, unmixing the MagXK record of biogenic reefs on various timescales offers an opportunity to test the roles of each factor (Figures 7 and 8).

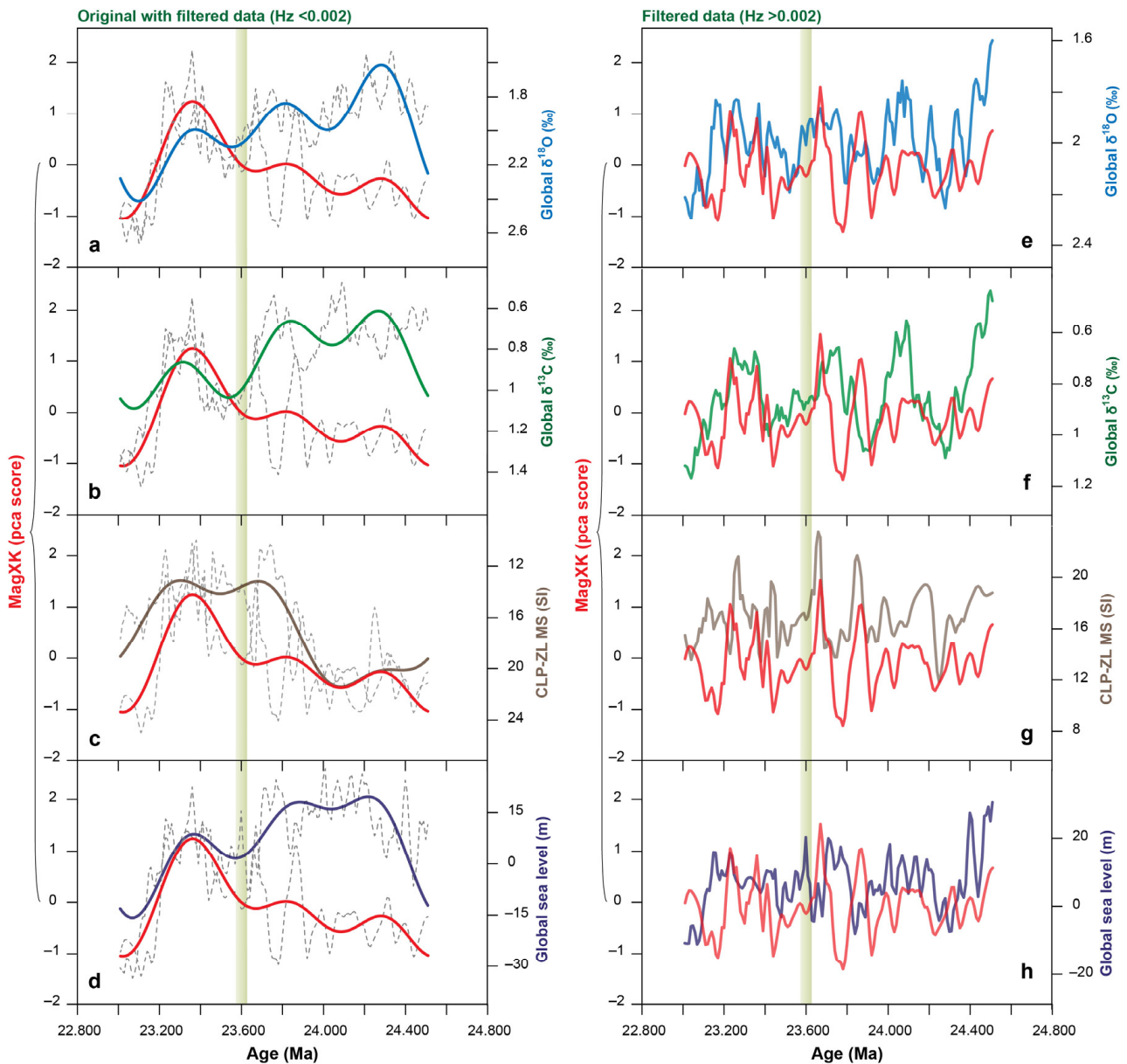


Figure 7. Comparison between the MagXK of core XK-1 and various paleoenvironmental proxies. (a–f) The MagXK of core XK-1 versus global $\delta^{18}\text{O}$ and $\delta^{13}\text{C}$ records [16]. (c,g) The MagXK versus the CLP-ZL MS, the loess magnetic susceptibility of Zhuanglang Profile in the Chinese Loess Plateau [61]. (d,h) The MagXK versus global sea level [62]. Dashed lines, original data; bold lines on the left panel, low-passed-filtered component (FFT filter, >0.5 Myr); lines on the right panel, high-passed-filtered component (FFT filter, <0.5 Myr).

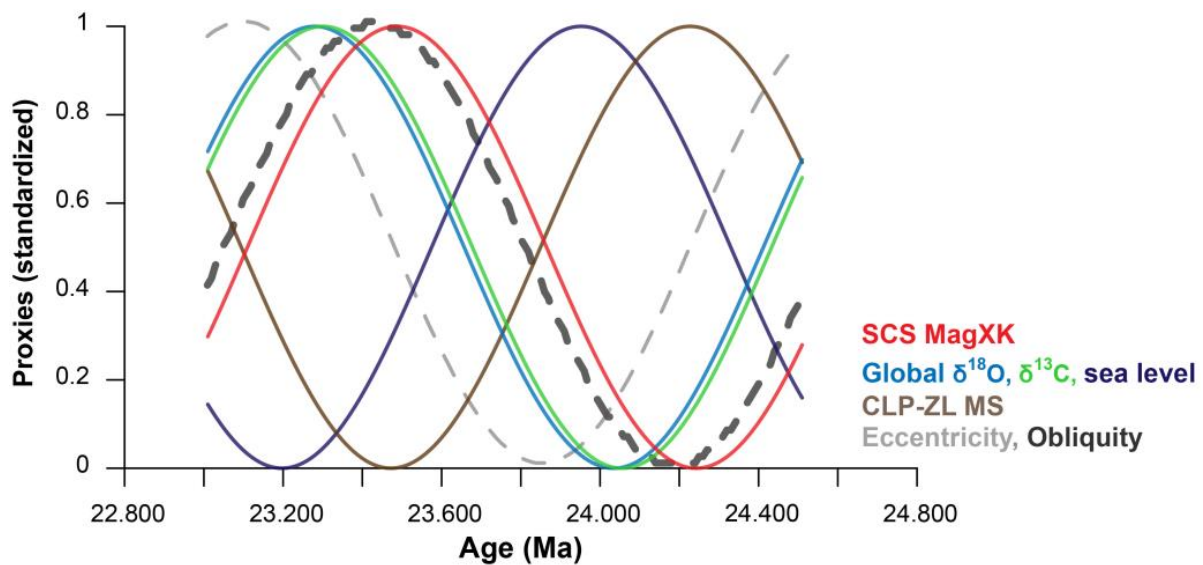


Figure 8. Comparison between paleoenvironmental proxies. All data were from low-passed-filtered components (FFT filter >1.0 Myr). See Figures 6 and 7.

As shown in a comparison between orbital eccentricity and the MagXK at the ~100 kyr band (Figure 6c), there is a transition around the Oligo–Miocene boundary. Additionally, in the early Miocene, the two records covaried at the 405 kyr band (Figure 6a). The changing relationship may infer a complex response of biogenic reefs at the very beginning to various environmental processes, and this is made evident by comparing this instance to other paleoenvironmental proxies (Figure 7).

For example, using $\delta^{18}\text{O}$ and $\delta^{13}\text{C}$ to indicate global temperature and CO_2 changes, respectively [16,63], the two key processes are closely correlated (Figure 7a,b). As a response to global climate change, on the ~0.5 Myr timescale, the MagXK record is positively correlated with global temperature changes ($\delta^{18}\text{O}$), indicating that biogenic reefs tend to decay in a cooler climate, while on the 0.5 Myr timescale, the MagXK is in-phase linked to global CO_2 changes ($\delta^{13}\text{C}$), suggesting that reef flourishing is in a higher CO_2 state. Similarly, the MagXK was positively correlated with the global sea level on the ~0.5 Myr timescale, suggesting that high sea-levels would not prevent reef developments, while on the 0.5 Myr timescale, it showed the opposite relationship (Figure 7d). Moreover, on the ~100–200 kyr timescales, the MagXK is generally correlated with global temperature and CO_2 changes ($\delta^{18}\text{O}$ and $\delta^{13}\text{C}$) (Figure 7e,f) as well as global sea level with some anti-phase intervals (Figure 7h).

Based on these observations, we present a complex relationship for the initiation of biogenic reefs in the South China Sea at the Oligo–Miocene boundary. In specific, on high-frequency variabilities, reef development in the South China Sea covaried with global temperature and CO_2 changes ($\delta^{18}\text{O}$ and $\delta^{13}\text{C}$) and sea levels. On a medium timescale, high temperature ($\delta^{18}\text{O}$), high sea level, and low CO_2 ($\delta^{13}\text{C}$) would induce biogenic reefs, and for long-term changes on the 0.5 Myr timescale, biogenic reefs were closely linked to low temperature ($\delta^{18}\text{O}$), low sea level, and high CO_2 ($\delta^{13}\text{C}$).

In modern studies, ocean acidification due to atmospheric CO_2 can significantly affect coral calcification rates, inhibit the development of coral larvae, and trigger the dissolution of coral reefs [64–68], and global warming with high sea levels can induce coral bleaching and inhibit self-renovation of coral reefs [4,6,14,69–71]. From a long-term perspective, our results may suggest a nonlinear and more complex response of reef development to global climate change, and this is also evident in modern observation. For example, corals can resist heat stress to a certain extent by changing the types of symbiotic algae and by regulating gene expression [72–74].

On the other hand, there are some offsets in these comparisons (Figure 7), likely suggesting that factors besides temperature, CO₂, and sea level changes played an important role in the initiation of biogenic reefs in the South China Sea. For example, based on dating carbonate in the Maldives, the South Asian monsoon was proposed to weakly begin at ~25 Ma with an abrupt onset at ~13 Ma [75]. Meanwhile, the East Asian monsoon similarly initiated in the late Oligocene [61,76]. In a comparison of the MagXK to monsoon changes inferred from the loess magnetic susceptibility of the Zhuanglang Profile in the Chinese Loess Plateau (CLP-ZL MS), a better but distinct agreement was observed in various timescales (Figure 7c,g). In specific, on the 0.5 Myr timescale, the MagXK is negatively correlated with the CLP-ZL MS record, while on the ~100–200 kyr timescales, a positive relationship is evident, confirming the reliability of the age-depth model within the study interval. Due to the anti-phase relationship between the East Asian summer and winter monsoons (e.g., [61,77]), it is inferred that the winter monsoon may be the dominant factor on the 0.5 Myr timescale while the summer monsoon may dominate on the ~100–200 kyr timescales.

In the Xisha (Paracel) Islands, the sea surface temperature is above 29 °C from May to September and below 24 °C in January, and thus, winter (from October to December) is the more favorable season for reef development [78]. Integrating all of this evidence, the link between biogenic reefs in the South China Sea and global climate change during 24.5–23.0 Ma was proposed as follows.

At the Oligo–Miocene boundary, subject to regional turbidity, temperature, and nutrients, coral reefs in the Caribbean, Central America, were extinct [79]. Meanwhile, due to tectonic subsidence, biogenic reefs initiated in the South China Sea [18,30] and in the Indian Ocean [75]. At the very beginning of biogenic reefs in the South China Sea, the growth intensity may be closely correlated to, or paced by, the East Asian winter monsoon on the 0.5 Myr timescales, and the reefs were likely linked to the East Asian summer monsoon on the ~100–200 kyr timescales. Since the reefs migrated seaward as sea levels fell (e.g., [80]), the positive relationship demonstrates that sea level is another important factor in reef development in the study area. However, there are many offsets between the MagXK and global sea level on the ~100–200 kyr timescales, implying the difference between global and regional sea-level changes, or that the influence of sea level may not have been consistent during the depositional period. For example, during 24.0–23.6 Ma and 23.2–23.0 Ma, high growth intensity indicated by the MagXK record was associated with sea-level low stands (Figure 7h). The anti-phase intervals between the MagXK and global sea level may highlight the influence of temperature and atmospheric CO₂. For global temperature and CO₂ changes, distinct influences were observed on various timescales, likely illustrating a self-adjustment process in the coral system. The relationship can be summarized: (1) high temperature and low CO₂ could induce reef developments on the ~0.5 Myr and ~100–200 kyr timescales, (2) low temperature with high CO₂ would pace biogenic reefs on the 0.5 Myr timescales, and the latter was similarly reported in tropical reefs in the last interglacial period [81]. It is noted that the correlations presented herein are based on the preliminary age model (Figure 2c), and high-frequency variabilities are usually more sensitive to the reliability of the age model. Thus, it is possible that the correlations on the ~100–200 kyr timescales could be modified in light of future research.

For long-term variabilities, orbital parameters have been proposed to be the major force on various paleoenvironmental processes on the Earth (e.g., [16,82,83]), and orbital obliquity is thought to be more important than previously assumed (e.g., [84,85]). In this study, on the 1.0 Myr timescales, the MagXK, the CLP-ZL MS, and orbital obliquity agree well with each other, while global temperature, CO₂, and sea level are coupled (Figure 8). This high similarity and in-phase variabilities between the MagXK, the CLP-ZL MS, and orbital obliquity may highlight the obliquity in pacing the initiation of the Asian monsoon and biogenic reefs in the South China Sea as the first-order force.

5. Conclusions

By studying the magnetic properties of biogenic reefs in core XK-1, drilled from the Xisha (Paracel) Islands, South China Sea, the detailed response of biogenic reefs to global climate change was revealed during the Oligo–Miocene transition. The main results are as follows: (1) magnetic minerals in the XK-1 biogenic reefs are dominated by low-coercivity and relatively coarse magnetite; (2) changes in magnetic parameters can be clustered into two sections at ~23.6 Ma, and the differences between the two units are evident. By stacking the concentration-dependent magnetic parameters (χ ARM and IRMs), a magnetic record indicating the development of biogenic reefs was derived. Based on this record, a complex relationship of biogenic reefs in response to global $\delta^{18}\text{O}$, $\delta^{13}\text{C}$, and sea level changes was observed. Moreover, biogenic reefs were also closely correlated or paced by the East Asian winter monsoon on the 0.5 Myr timescales. Therefore, there is a close link between biogenic reef evolution in the Xisha Islands and global climate change during the Oligo–Miocene boundary, and the origin was likely paced by orbital obliquity on long-term timescales. However, the age model of core XK-1 was only based on magnetostratigraphy and the relationship between reef growth and magnetic properties has not been supported by modern observations. Investigation about these two keys are worthy of further studies in the future.

Author Contributions: Conceptualization and methodology, L.Y.; sample collection, X.L.; formal analysis, Y.L. and W.C.; original draft preparation, X.L. and L.Y. All authors have read and agreed to the published version of the manuscript.

Funding: This research was funded by the National Key R&D Program of China (2018YFE0202401), the National Natural Science Foundation of China (42177422), and the Global Changing and Air-sea Interaction (GASI-GEOGE-04).

Institutional Review Board Statement: Not applicable.

Informed Consent Statement: Not applicable.

Data Availability Statement: All magnetic data presented in this work can be obtained from L.Y. (yiliang@tongji.edu.cn) and have been stored in an online repository (https://mda.vliz.be/directlink.php?fid=VLIZ_00000824_613746d253ee3437877792) ‘Marine Data Archive’.

Acknowledgments: We thank Chenglong Deng at the Institute of Geology and Geophysics, Chinese Academy of Sciences, for help with this study and Xiaoke Qiang at the Institute of Earth Environment, Chinese Academy of Sciences, for sharing the loess data of the Zhuanglang Profile.

Conflicts of Interest: The authors declare no conflict of interest.

References

1. Milliman, J.D. Production and accumulation of calcium carbonate in the ocean: Budget of a nonsteady state. *Glob. Biogeochem. Cycles* **1993**, *7*, 927–957. [[CrossRef](#)]
2. Milliman, J.D.; Drozler, A.W. Neritic and pelagic carbonate sedimentation in the marine environment: Ignorance is not bliss. *Geol. Rundsch.* **1996**, *85*, 496–504. [[CrossRef](#)]
3. Eyre, B.D.; Andersson, A.J.; Cyronak, T. Benthic coral reef calcium carbonate dissolution in an acidifying ocean. *Nat. Clim. Chang.* **2014**, *4*, 969–976. [[CrossRef](#)]
4. Hoegh-Guldberg, O.; Mumby, P.J.; Hooten, A.J.; Steneck, R.S.; Greenfield, P.; Gomez, E.; Harvell, C.D.; Sale, P.F.; Edwards, A.J.; Caldeira, K.; et al. Coral reefs under rapid climate change and ocean acidification. *Science* **2007**, *318*, 1737–1742. [[CrossRef](#)]
5. Hughes, T.P.; Kerry, J.T.; Álvarez-Noriega, M.; Álvarez-Romero, J.G.; Anderson, K.D.; Baird, A.H.; Babcock, R.C.; Beger, M.; Bellwood, D.R.; Berkelmans, R.; et al. Global warming and recurrent mass bleaching of corals. *Nature* **2017**, *543*, 373–377. [[CrossRef](#)] [[PubMed](#)]
6. Pandolfi, J. Incorporating Uncertainty in Predicting the Future Response of Coral Reefs to Climate Change. *Annu. Rev. Ecol. Evol. Syst.* **2015**, *46*, 281–303. [[CrossRef](#)]
7. Cumming, G.S.; Morrison, T.H.; Hughes, T.P. New Directions for Understanding the Spatial Resilience of Social–Ecological Systems. *Ecosystems* **2017**, *20*, 649–664. [[CrossRef](#)]
8. Levin, S.; Xepapadeas, T.; Crépin, A.-S.; Norberg, J.; de Zeeuw, A.; Folke, C.; Hughes, T.; Arrow, K.; Barrett, S.; Daily, G.; et al. Social-ecological systems as complex adaptive systems: Modeling and policy implications. *Environ. Dev. Econ.* **2012**, *18*, 111–132. [[CrossRef](#)]

9. Fischer, J.; Gardner, T.A.; Bennett, E.M.; Balvanera, P.; Biggs, R.; Carpenter, S.; Daw, T.; Folke, C.; Hill, R.; Hughes, T.P.; et al. Advancing sustainability through mainstreaming a social–ecological systems perspective. *Curr. Opin. Environ. Sustain.* **2015**, *14*, 144–149. [[CrossRef](#)]
10. Martin, R.; Schlüter, M. Combining system dynamics and agent-based modeling to analyze social-ecological interactions—an example from modeling restoration of a shallow lake. *Front. Environ. Sci.* **2015**, *3*, 66. [[CrossRef](#)]
11. Laborde, S.; Fernández, A.; Phang, S.C.; Hamilton, I.M.; Henry, N.; Jung, H.C.; Mahamat, A.; Ahmadou, M.; Labara, B.K.; Kari, S.; et al. Social-ecological feedbacks lead to unsustainable lock-in in an inland fishery. *Glob. Environ. Chang.* **2016**, *41*, 13–25. [[CrossRef](#)]
12. Figueiredo, J.; Pereira, H.M. Regime shifts in a socio-ecological model of farmland abandonment. *Landsch. Ecol.* **2011**, *26*, 737–749. [[CrossRef](#)]
13. Ban, S.S.; Graham, N.A.J.; Connolly, S.R. Evidence for multiple stressor interactions and effects on coral reefs. *Glob. Chang. Biol.* **2014**, *20*, 681–697. [[CrossRef](#)] [[PubMed](#)]
14. Hughes, T.P.; Barnes, M.L.; Bellwood, D.R.; Cinner, J.E.; Cumming, G.S.; Jackson, J.B.C.; Kleypas, J.; van de Leemput, I.A.; Lough, J.M.; Morrison, T.H.; et al. Coral reefs in the Anthropocene. *Nature* **2017**, *546*, 82–90. [[CrossRef](#)] [[PubMed](#)]
15. Quattrini, A.M.; Rodríguez, E.; Faircloth, B.C.; Cowman, P.F.; Brugler, M.R.; Farfan, G.A.; Hellberg, M.E.; Kitahara, M.V.; Morrison, C.L.; Paz-García, D.A.; et al. Palaeoclimate ocean conditions shaped the evolution of corals and their skeletons through deep time. *Nat. Ecol. Evol.* **2020**, *4*, 1531–1538. [[CrossRef](#)] [[PubMed](#)]
16. Zachos, J.; Pagani, M.; Sloan, L.; Thomas, E.; Billups, K. Trends, Rhythms, and Aberrations in Global Climate 65 Ma to Present. *Science* **2001**, *292*, 686–693. [[CrossRef](#)] [[PubMed](#)]
17. Wu, S.; Yang, Z.; Wang, D.; Lü, F.; Lüdmann, T.; Fulthorpe, C.; Wang, B. Architecture, development and geological control of the Xisha carbonate platforms, northwestern South China Sea. *Mar. Geol.* **2014**, *350*, 71–83. [[CrossRef](#)]
18. Yi, L.; Jian, Z.; Liu, X.; Zhu, Y.; Zhang, D.; Wang, Z.; Deng, C. Astronomical tuning and magnetostratigraphy of Neogene biogenic reefs in Xisha Islands, South China Sea. *Sci. Bull.* **2018**, *63*, 564–573. [[CrossRef](#)]
19. Fulthorpe, C.S.; Schlanger, S.O. Paleo-oceanographic and tectonic setting of Early Miocene reefs and associated carbonates offshore Southeast Asia. *AAPG Bull.* **1989**, *73*, 729–756.
20. Sales, A.O.; Jacobsen, E.C.; Morado Jr, A.A.; Benavidez, J.J.; Navarro, F.A.; Lim, A.E. The petroleum potential of deep-water northwest Palawan Block GSEC 66. *J. Asian Earth Sci.* **1997**, *15*, 217–240. [[CrossRef](#)]
21. Williams, H.H. Play concepts-northwest Palawan, Philippines. *J. Asian Earth Sci.* **1997**, *15*, 251–273. [[CrossRef](#)]
22. Hutchison, C.S. Marginal basin evolution: The southern South China Sea. *Mar. Pet. Geol.* **2004**, *21*, 1129–1148. [[CrossRef](#)]
23. Hutchison, C.S.; Vijayan, V.R. What are the Spratly Islands? *J. Asian Earth Sci.* **2010**, *39*, 371–385. [[CrossRef](#)]
24. Ma, Y.; Wu, S.; Lv, F.; Dong, D.; Sun, Q.; Lu, Y.; Gu, M. Seismic characteristics and development of the Xisha carbonate platforms, northern margin of the South China Sea. *J. Asian Earth Sci.* **2011**, *40*, 770–783. [[CrossRef](#)]
25. Yi, L.; Wang, Z.; Zhang, D.; Liu, X.; You, L.; Luo, W.; Zhu, Y.; Qin, H.; Deng, C. Magnetostratigraphy of biogenic reefs in the Sanya Formation of Borehole XK-1 from Xisha Islands and its environmental significance. *Coast. Eng.* **2016**, *35*, 1–11. (In Chinese)
26. Zhang, M.S.; He, Q.X.; Ye, Z.J. *The Geologic Research of Deposition of Bioherm Carbonate in the Xisha Islands*; Science Press: Beijing, China, 1989.
27. Zhao, H.T.; Sha, Q.A.; Zhu, Y.Z. *Quaternary Coral Reef: Geology of Yongshu Reef, Nansha Islands*; China Ocean Press: Beijing, China, 1992; p. 264.
28. Zhu, Y.Z.; Sha, Q.A.; Guo, L.F.; Yu, K.F.; Zhao, H.T. *Cenozoic Coral Reef Geology of Yongshu Reef, Nansha Islands*; Science Press: Beijing, China, 1997; p. 137.
29. Xu, S.; Yu, K.; Fan, T.; Jiang, W.; Wang, R.; Zhang, Y.; Yue, Y.; Wang, S. Coral reef carbonate $\delta^{13}\text{C}$ records from the northern South China Sea: A useful proxy for seawater $\delta^{13}\text{C}$ and the carbon cycle over the past 1.8 Ma. *Glob. Planet. Chang.* **2019**, *182*, 103003. [[CrossRef](#)]
30. Yi, L.; Deng, C.; Yan, W.; Wu, H.; Zhang, C.; Xu, W.; Su, X.; He, H.; Guo, Z. Neogene–quaternary magnetostratigraphy of the biogenic reef sequence of core NK-1 in Nansha Qundao, South China Sea. *Sci. Bull.* **2021**, *66*, 200–203. [[CrossRef](#)]
31. Qiao, P.; Zhu, W.; Shao, L.; Zhang, D.; Cheng, X.; Song, Y. Carbonate stable isotope stratigraphy of Well Xike-1, Xisha Islands. *J. China Univ. Geosci.* **2015**, *40*, 725–732. [[CrossRef](#)]
32. Wang, Z.; Zhang, D.; Liu, X.; You, L.; Luo, W.; Yi, L.; Zhu, Y.; Qin, H.; Xie, Q.; Che, Z.; et al. Preliminary results of rock magnetism and magnetostratigraphy for Late Miocene to Pliocene biogenic reefs in the Xisha Islands, South China Sea. *Chin. J. Geophys.* **2016**, *59*, 4178–4187. [[CrossRef](#)]
33. Lund, S.; Platzman, E.; Thouveny, N.; Camoin, G.; Corsetti, F.; Berelson, W. Biological control of paleomagnetic remanence acquisition in carbonate framework rocks of the Tahiti coral reef. *Earth Planet. Sci. Lett.* **2010**, *298*, 14–22. [[CrossRef](#)]
34. Wei, X.; Deng, J.F.; Xie, W.Y.; Zhu, Y.J.; Zhao, G.C.; Li, Y.X.; Chen, Y.H. Constraints on biogenetic reef formation during evolution of the South China Sea and exploration potential analysis. *Earth Geosci. Front.* **2005**, *12*, 245–252.
35. Wang, P.; Li, Q. *The South China Sea: Paleooceanography and Sedimentology*; Springer: Dordrecht, The Netherlands, 2009; Volume 13, p. 506.
36. Xu, G.Q.; Lv, B.Q.; Wang, H.G. Drown event research: Insight from Cenozoic carbonate platform in northern South China Sea. *J. Tongji Univ.* **2002**, *30*, 35–40.

37. Fyhn, M.B.W.; Boldreel, L.O.; Nielsen, L.H.; Giang, T.C.; Nga, L.H.; Hong, N.T.M.; Nguyen, N.D.; Abatzis, I. Carbonate platform growth and demise offshore Central Vietnam: Effects of Early Miocene transgression and subsequent onshore uplift. *J. Asian Earth Sci.* **2013**, *76*, 152–168. [[CrossRef](#)]
38. Zhu, W.; Wang, Z.; Mi, L.; Du, X.; Xie, X.; Lu, Y.; Zhang, D.; Sun, Z.; Liu, X.; You, L. Sequence stratigraphic framework and reef growth unit of Well Xike-1 from Xisha Islands, South China Sea. *J. China Univ. Geosciences* **2015**, *40*, 677–687.
39. Luo, W.; Zhang, D.; Liu, X.; Wang, Z.; Hu, W.; Wang, Y. A comprehensive stratigraphic study of Well XK-1 in the Xisha Area. *J. Stratigr.* **2018**, *42*, 485–498.
40. Wang, Z.; Zhang, D.; Liu, X.; You, L.; Luo, W.; Yi, L.; Tan, L.; Zhu, Y.; Qin, H.; Cheng, H.; et al. Magnetostratigraphy and 230Th dating of Pleistocene biogenic reefs in XK-1 borehole from Xisha Islands, South China Sea. *Chin. J. Geophys.* **2017**, *60*, 1027–1038. (In Chinese) [[CrossRef](#)]
41. Wu, F.; Xie, X.; Zhu, Y.; Chen, B.; Shang, Z. Sequence stratigraphy of the Late Oligocene carbonate system on the Xisha Islands in the South China Sea. *Int. J. Earth Sci.* **2021**, *110*, 1611–1629. [[CrossRef](#)]
42. Tauxe, L. *Essentials of Paleomagnetism*; University of California Press: Berkeley, CA, USA, 2010.
43. Heslop, D. Numerical strategies for magnetic mineral unmixing. *Earth-Sci. Rev.* **2015**, *150*, 256–284. [[CrossRef](#)]
44. Heslop, D.; Roberts, A.P. Unmixing Magnetic Hysteresis Loops. *J. Geophys. Res. Atmos.* **2012**, *117*, 3758. [[CrossRef](#)]
45. Kletetschka, G.; Schnabl, P.; Šifnerová, K.; Tasáryová, Z.; Manda, Š.; Pruner, P. Magnetic scanning and interpretation of paleomagnetic data from Prague Synform's volcanics. *Studia Geophys. Geod.* **2013**, *57*, 103–117. [[CrossRef](#)]
46. Duan, Z.; Gao, X.; Liu, Q. Anhyseretic remanent magnetization (ARM) and its application to geoscience. *Prog. Geophys.* **2012**, *27*, 1929–1938. [[CrossRef](#)]
47. Maher, B.A. Magnetic properties of some synthetic sub-micron magnetites. *Geophys. J.* **1988**, *94*, 83–96. [[CrossRef](#)]
48. Evans, M.E.; Heller, F. *Environmental Magnetism: Principles and Applications of Enviromagnetics*; Academic Press: New York, NY, USA, 2003; p. 322.
49. Yi, L.; Wang, H.; Liu, G.; Chen, Y.; Yao, H.; Deng, X. Magnetic minerals in Mid-Pleistocene sediments on the Caiwei Guyot, Northwest Pacific and their response to the Mid-Brunhes climate event. *Acta Oceanol. Sin.* **2021**, *40*, 253.
50. Yang, D.; Wang, M.; Lu, H.; Ding, Z.; Liu, J.; Yan, C. Magnetic properties and correlation with heavy metals in mangrove sediments, the case study on the coast of Fujian, China. *Mar. Pollut. Bull.* **2019**, *146*, 865–873. [[CrossRef](#)] [[PubMed](#)]
51. Zhang, W.; Appel, E.; Fang, X.; Song, C.; Cirpka, O. Magnetostratigraphy of deep drilling core SG-1 in the western Qaidam Basin (NE Tibetan Plateau) and its tectonic implications. *Quat. Res.* **2012**, *78*, 139–148. [[CrossRef](#)]
52. Roberts, A.P.; Heslop, D.; Zhao, X.; Pike, C.R. Understanding fine magnetic particle systems through use of first-order reversal curve diagrams. *Rev. Geophys.* **2014**, *52*, 557–602. [[CrossRef](#)]
53. Roberts, A.P.; Pike, C.R.; Verosub, K.L. First-order reversal curve diagrams: A new tool for characterizing the magnetic properties of natural samples. *J. Geophys. Res. Solid Earth* **2000**, *105*, 28461–28475. [[CrossRef](#)]
54. Wang, X.; Wang, Y.; Liu, J.; Zhang, D.; Li, X.; Shi, Z. Characteristics and significance of manganese minerals in dolostones from Well Xike-1, Xisha Area, South China Sea. *Mineral. Petrol.* **2020**, *40*, 81–91.
55. Laskar, J.; Fienga, A.; Gastineau, M.; Manche, H. La2010: A new orbital solution for the long-term motion of the Earth. *Astron. Astrophys.* **2011**, *532*, A89. [[CrossRef](#)]
56. Grinsted, A.; Moore, J.C.; Jevrejeva, S. Application of the cross wavelet transform and wavelet coherence to geophysical time series. *Nonlinear Process. Geophys.* **2004**, *11*, 561–566. [[CrossRef](#)]
57. Bachtel, S.L.; Kissling, R.D.; Martono, D.; Rahardjanto, S.P.; Dunn, P.A.; MacDonald, B.A. Seismic Stratigraphic Evolution of the Miocene–Pliocene Segitiga Platform, East Natuna Sea, Indonesia: The Origin, Growth Ad Demise of an Isolated Carbonate Platform. In *Seismic Imaging of Carbonate Reservoir and Systems*; Eberli, G.P., Massafiero, J.L., Sarg, J.F., Eds.; AAPG Memoir: Tulsa, OK, USA, 2003; Volume 81, pp. 309–328.
58. Belopolsky, A.V.; Droxler, A.W. Imaging Tertiary carbonate systems, the Maldives, Indian Ocean: Insights into carbonate sequence interpretation. *Lead. Edge* **2003**, *22*, 646–652. [[CrossRef](#)]
59. Epting, M. The Miocene carbonate buildups of central Luconia, offshore Sarawak. In *Atlas of Seismic Stratigraphy*; Bally, A.W., Ed.; AAPG: Tulsa, OK, USA, 1989; pp. 168–173.
60. Wilson, M.E.J. Cenozoic carbonates in Southeast Asia: Implications for equatorial carbonate development. *Sediment. Geol.* **2002**, *147*, 295–428. [[CrossRef](#)]
61. Qiang, X.; An, Z.; Song, Y.; Chang, H.; Sun, Y.; Liu, W.; Ao, H.; Dong, J.; Fu, C.; Wu, F.; et al. New eolian red clay sequence on the western Chinese Loess Plateau linked to onset of Asian desertification about 25 Ma ago. *Sci. China Earth Sci.* **2011**, *54*, 136–144. [[CrossRef](#)]
62. Miller, K.G.; Browning, J.V.; Schmelz, W.J.; Kopp, R.E.; Mountain, G.S.; Wright, J.D. Cenozoic sea-level and cryospheric evolution from deep-sea geochemical and continental margin records. *Sci. Adv.* **2020**, *6*, eaaz1346. [[CrossRef](#)] [[PubMed](#)]
63. Lisiecki, L.E. A benthic $\delta^{13}\text{C}$ -based proxy for atmospheric pCO₂ over the last 1.5 Myr. *Geophys. Res. Lett.* **2010**, *37*, L21708. [[CrossRef](#)]
64. Crook, E.D.; Cohen, A.L.; Rebolledo-Vieyra, M.; Hernandez, L.; Paytan, A. Reduced calcification and lack of acclimatization by coral colonies growing in areas of persistent natural acidification. *Proc. Natl. Acad. Sci. USA* **2013**, *110*, 11044–11049. [[CrossRef](#)] [[PubMed](#)]

65. Fantazzini, P.; Mengoli, S.; Pasquini, L.; Bortolotti, V.; Brizi, L.; Mariani, M.; Di Giosia, M.; Fermani, S.; Capaccioni, B.; Caroselli, E.; et al. Gains and losses of coral skeletal porosity changes with ocean acidification acclimation. *Nat. Commun.* **2015**, *6*, 7785. [[CrossRef](#)] [[PubMed](#)]
66. Mollica, N.R.; Guo, W.; Cohen, A.L.; Huang, K.F.; Foster, G.L.; Donald, H.K.; Solow, A.R. Ocean acidification affects coral growth by reducing skeletal density. *Proc. Natl. Acad. Sci. USA* **2018**, *115*, 1754–1759. [[CrossRef](#)] [[PubMed](#)]
67. Tambutté, E.; Venn, A.A.; Holcomb, M.; Segonds, N.; Techer, N.; Zoccola, D.; Allemand, D.; Tambutté, S. Morphological plasticity of the coral skeleton under CO₂-driven seawater acidification. *Nat. Commun.* **2015**, *6*, 7368. [[CrossRef](#)]
68. Foster, T.; Falter, J.; McCulloch, M.; Clode, P. Ocean acidification causes structural deformities in juvenile coral skeletons. *Sci. Adv.* **2016**, *2*, e1501130. [[CrossRef](#)]
69. Frölicher, T.L.; Fischer, E.M.; Gruber, N. Marine heatwaves under global warming. *Nature* **2018**, *560*, 360–364. [[CrossRef](#)] [[PubMed](#)]
70. Smale, D.A.; Wernberg, T.; Oliver, E.C.J.; Thomsen, M.; Harvey, B.P.; Straub, S.C.; Burrows, M.T.; Alexander, L.V.; Benthuyzen, J.A.; Donat, M.G.; et al. Marine heatwaves threaten global biodiversity and the provision of ecosystem services. *Nat. Clim. Chang.* **2019**, *9*, 306–312. [[CrossRef](#)]
71. Hughes, T.P.; Anderson, K.D.; Connolly, S.R.; Heron, S.F.; Kerry, J.T.; Lough, J.M.; Baird, A.H.; Baum, J.K.; Berumen, M.L.; Bridge, T.C.; et al. Spatial and temporal patterns of mass bleaching of corals in the Anthropocene. *Science* **2018**, *359*, 80–83. [[CrossRef](#)]
72. Enochs, I.C.; Manzello, D.P.; Donham, E.M.; Kolodziej, G.; Okano, R.; Johnston, L.; Young, C.; Iguel, J.; Edwards, C.B.; Fox, M.D.; et al. Shift from coral to macroalgae dominance on a volcanically acidified reef. *Nat. Clim. Chang.* **2015**, *5*, 1083–1088. [[CrossRef](#)]
73. Albright, R.; Caldeira, L.; Hofelt, J.; Kwiatkowski, L.; Maclaren, J.K.; Mason, B.M.; Nebuchina, Y.; Ninokawa, A.; Pongratz, J.; Ricke, K.L.; et al. Reversal of ocean acidification enhances net coral reef calcification. *Nature* **2016**, *531*, 362–365. [[CrossRef](#)] [[PubMed](#)]
74. Cooper, T.; O’Leary, R.; Lough, J. Growth of Western Australian Corals in the Anthropocene. *Science* **2012**, *335*, 593–596. [[CrossRef](#)]
75. Betzler, C.; Eberli, G.P.; Kroon, D.; Wright, J.D.; Swart, P.K.; Nath, B.N.; Alvarez-Zarikian, C.A.; Alonso-García, M.; Bialik, O.M.; Blättler, C.L.; et al. The abrupt onset of the modern South Asian Monsoon winds. *Sci. Rep.* **2016**, *6*, 29838. [[CrossRef](#)]
76. Guo, Z.; Ruddiman, W.F.; Hao, Q.; Wu, H.; Qiao, Y.; Zhu, R.; Peng, S.; Wei, J.J.; Yuan, B.; Liu, T.S. Onset of Asian desertification by 22 Myr ago inferred from loess deposits in China. *Nature* **2002**, *416*, 159–163. [[CrossRef](#)] [[PubMed](#)]
77. Sun, Y.; Clemens, S.C.; An, Z.; Yu, Z. Astronomical timescale and palaeoclimatic implication of stacked 3.6-Myr monsoon records from the Chinese Loess Plateau. *Quat. Sci. Rev.* **2006**, *25*, 33–48. [[CrossRef](#)]
78. Huang, H.; Dong, Z.; Lian, J. Establishment of nature reserve of coral reef ecosystem on the Xisha Islands. *Trop. Geogr.* **2008**, *28*, 540–544.
79. Edinger, E.N.; Risk, M.J. Oligocene-Miocene extinction and geographic restriction of Caribbean corals: Roles of turbidity, temperature, and nutrients. *Palaios* **1994**, *9*, 576–598. [[CrossRef](#)]
80. Webster, J.M.; Braga, J.C.; Humblet, M.; Potts, D.C.; Iryu, Y.; Yokoyama, Y.; Fujita, K.; Bourillot, R.; Esat, T.M.; Fallon, S.; et al. Response of the Great Barrier Reef to sea-level and environmental changes over the past 30,000 years. *Nat. Geosci.* **2018**, *11*, 426–432. [[CrossRef](#)]
81. Kiessling, W.; Simpson, C.; Beck, B.; Mewis, H.; Pandolfi, J.M. Equatorial decline of reef corals during the last Pleistocene interglacial. *Proc. Natl. Acad. Sci. USA* **2012**, *109*, 21378–21383. [[CrossRef](#)] [[PubMed](#)]
82. Cheng, H.; Edwards, R.L.; Sinha, A.; Spötl, C.; Yi, L.; Chen, S.; Kelly, M.; Kathayat, G.; Wang, X.; Li, X.; et al. The Asian monsoon over the past 640,000 years and ice age terminations. *Nature* **2016**, *534*, 640–646. [[CrossRef](#)] [[PubMed](#)]
83. Gradstein, F.M.; Ogg, J.G.; Schmitz, M.D.; Ogg, G.M. *Geologic Time Scale 2020*; Elsevier: Amsterdam, The Netherlands, 2020; p. 1357. [[CrossRef](#)]
84. Naish, T.; Powell, R.; Levy, R.; Wilson, G.; Scherer, R.; Talarico, F.; Krissek, L.; Niessen, F.; Pompilio, M.; Wilson, T. Obliquity-paced Pliocene West Antarctic ice sheet oscillations. *Nature* **2009**, *458*, 322–328. [[CrossRef](#)] [[PubMed](#)]
85. Huang, H.; Gao, Y.; Ma, C.; Jones, M.M.; Zeeden, C.; Ibarra, D.E.; Wu, H.; Wang, C. Organic carbon burial is paced by a ~173-ka obliquity cycle in the middle to high latitudes. *Sci. Adv.* **2021**, *7*, eabf9489. [[CrossRef](#)]